Electronic Supplementary Information (ESI)

Encapsulating V_2O_5 into Carbon Nanotube Enables Flexible High-Performance Lithium Ion Batteries

Debin Kong,[a,b] Xianglong Li,[b] Yunbo Zhang,[b] Xiao Hai,[b] Bin Wang,[b] Xiongying Qiu,[b] Qi Song,[b] Quan-Hong Yang[a] and Linjie Zhi[a,b]**

[a] *School of Chemical Engineering and Technology, Tianjin University, Tianjin, 300072 (China)*
[b] *CAS Key Laboratory of Nanosystem and Hierarchical Fabrication, CAS Center for Excellence in Nanoscience, National Center for Nanoscience and Technology, Beijing 100190, China*
E-mail: zhilj@nanoctr.cn, qhyangcn@tju.edu.cn

Experimental Section:

Typical procedure for V_2O_5@G preparation: First, a flexible film composed by V-SiO_2-PVP is produced through electrospinning of 4 ml DMF solution of 0.4 g PVP with the addition of 0.36 g Vanadium oxide sulfate ($VOSO_4$) and 500 μL TEOS. A voltage of 17 kV was applied to the solution to start the spinning process with a high voltage source (SL50P60, Spellman High Voltage Electronics Corporation). A flat Al foil covered with non-dust cloth was placed at a distance of 13 cm away from the needle as a sample collector. Afterward, the resulting film was heated to 1070 ^{o}C at a rate of 10 ^{o}C min^{-1} in a horizontal tube furnace under argon/hydrogen (Ar/H_2; 2:1) atmosphere. Then, 100 sccm methane (CH_4) was introduced into the reaction tube and kept for 5 min. After that, the sample was rapidly cooled down to room temperature under the protection of Ar and H_2, resulting in several layers of graphitic carbon encapsulation with good mechanical properties and excellent conductivity. Subsequently, V_2O_5@G is finally obtained by annealing at 376 ℃ in the air via a three gradient temperature program after the removal of SiO_2 by HF. The samples containing different V_2O_5 mass ratio were prepared from electrospinning solutions with different $VOSO_4$ concentration.

Typical procedure for V_2O_5/G preparation: First, a film consisted of graphene nanotube is obtained (**Figure S9**), which is similar to V_2O_5@G, excepting that no V source ($VOSO_4$) is added. Then, it was dispersed fully into 40 mL of an anhydrous ethanol solution and ultrasonicated for another 40 min. After that, 300 μL of vanadium oxytripropoxide (VOTP; 99% purity, Aldrich) was added dropwise into the above solution. Finally, the resulting mixed solution was transferred into a 100-mL Teflon-lined stainless steel autoclave and kept at 160°C for 12 h. V_2O_5/G is finally obtained by annealing at 360 ℃ in the air via a three gradient temperature program

Characterization: The morphologies of the samples were examined by the scanning electron microscope (Hitachi S4800) and field emission transmission electron microscopy (FEI Tecnai G^2 20 ST). X-ray diffraction (XRD) with Cu Kα radiation (Rigaku D/max-2500B2+/PCX system) was used to determine the phase composition and the crystallinity.

Electrochemical characterization. Both the free-standing V_2O_5@G and V_2O_5/G film was directly used as the working electrode. The as-made working electrodes were assembled into coin-type half cells (CR2032) in an argon-filled glovebox (<1 ppm of oxygen and water) with lithium foil as the counter electrode, porous polypropylene film as the separator, and 1M $LiPF_6$ in 1:1 (v/v) ethylene carbonate/diethyl carbonate (EC/DEC) as the electrolyte. Notably, the obtained V_2O_5@G film was directly used as the electrode without any current collector and binder. For each investigated electrode, the total electrode weight (the weight of V_2O_5@G film including graphene) were used for calculating specific capacities. The total mass of V_2O_5@G film applied to each cell was around 1.5~2.0 mg cm^{-2}. The cycle-life tests were performed using a CT2001A battery program controlling test system at different current rates within the 2V - 4V voltage range. For achieving the capacity values of each electrode material, at least three cells were assembled and characterized under the same conditions. For each investigated electrode, the total electrode weight were used for calculating specific capacities. As for the full cell fabrication, the pre-lithiation process is achieved through an electrochemical method via Electrochemical Station in an argon-filled glovebox. Similar to half cells assembling, SnOx@G is used as the positive electrode with lithium foil as the counter electrode, porous polypropylene film as the separator. The current density is 0.1 A g-1 and the cut off voltage is 0.01 V. The optimized mass ratio of the cathodes and anodes is 5 mg : 2 mg (the anode capacity excesses 15- 20%).

Table S1 A collection of the electrochemical properties of V_2O_5-based cathodes based on the whole electrode

Electrode description	**Cited literature**	**V_2O_5 (%)**	**capacity based on the whole electrode (mAh/g)**	**current density based on the whole electrode (A/g)**
yolk–shell V_2O_5	1	60	162.6	0.6
cucumber-like V_2O_5/poly(3,4-ethylenedioxythiophene)&MnO_2	2	70	33.6	0.35
graphene nanoribbon/V_2O_5 cathodes	3	34	56.1	0.21
2D V_2O_5 sheet network	4	70	115.5	0.7
interconnected V_2O_5 nanosheets assembled on carbon nanotube	5	58	67.4	5.81
carbon-coated V_2O_5 nanocrystals	6	60	78	6
rattle-type V_2O_5 hollow microspheres	7	70	88.9	1.68
hierarchical V_2O_5 hollow microspheres	8	67.60	112.2	1.62

leaf-like V_2O_5 nanosheets	9	75	86.3	3.75
V_2O_5-glycolate hollow microspheres	10	70	87.5	1.68
nanowire templated semihollow bicontinuous grapheme/V_2O_5 scrolls	11	75	121.5	2.25
uniform V_2O_5 nanosheet-assembled hollow microflowers	12	75	57	0.75
single crystalline V_2O_5 nanowires / graphene composite	13	76.88	84.6	1.23
V_2O_5 microspheres	14	70	119	1.68
V_2O_5 /Conductive Polymer Core/Shell Nanobelt Array on Three Dimensional Graphite Foam	15	53.56	61.6	12.8

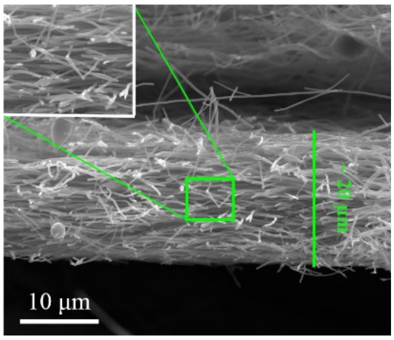

Figure S1. The SEM cross section image of our V_2O_5@G

The electrical conductivity of our V_2O_5@G electrode and the film thickness are measured by electronic thickness gauge. The self-supported film holds a resistance of around 730 $\Omega\ \square^{-1}$, and a thickness of ca. 20 μm, resulting in an electrical conductivity of 0.7 S cm^{-1}, which is more than three orders of magnitude compared with that of the bulk V_2O_5 (10^{-4}~10^{-5} S cm^{-1}).[16, 17] The SEM cross section images (Figure S1) further proves the film thickness of around 20 μm.

Figure S2. The optical images of our materials under a 7 mm cubic 4.5 g weigh object.

The material can keep well shaped under a 7 mm cubic 4.5g weigh object which delivers a pressure of around 10^3 Pa. This result suggest that the flexible electrode developed in this work holds enough mechanical strength for processing and mass-scale production

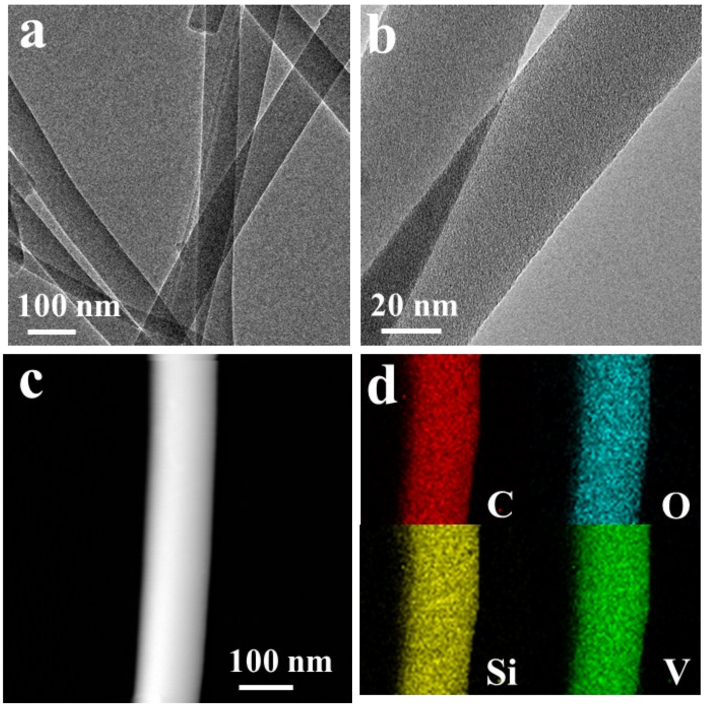

Figure S3. The TEM results of the sample after annealing to 1070℃ without the presence of methane. (a) The TEM photos. scale bar, 100 nm; (b) The TEM photos. scale bar, 20 nm; (c) Dark field transmission electron microscopy image. Scale bar, 100 nm; (d) Carbon, Silicon, Oxygen and Vanadium elemental mapping of a selected area of an individual V_2O_5@G.

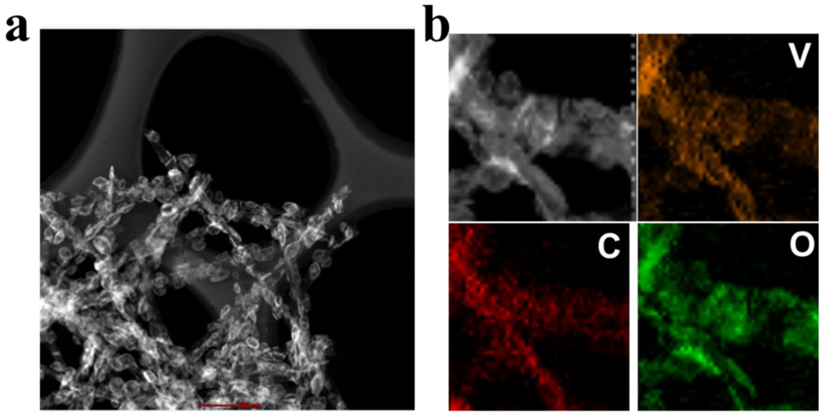

Figure S4. (a) Dark field transmission electron microscopy image of V_2O_5/G. Scale bar, 500 nm; (b) Vanadium, Oxygen and Carbon elemental mapping of a selected area of an individual V_2O_5/G.

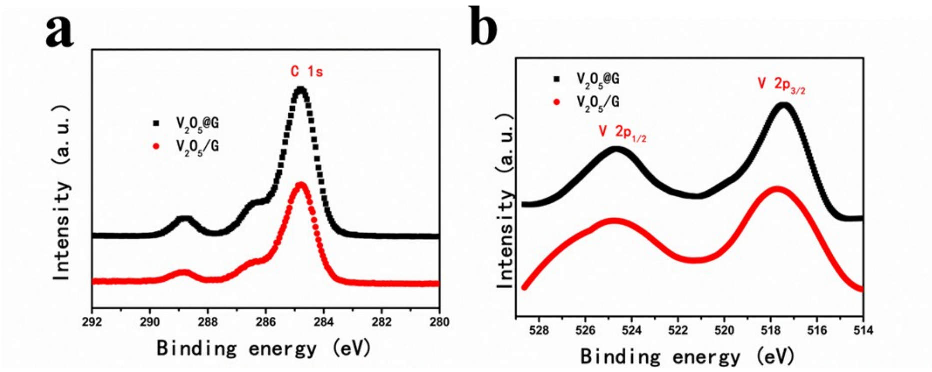

Figure S5. a) Survey XPS spectrum of V_2O_5@G and V_2O_5/G. (b) XPS spectrum of the V 2p binding energy region showing spin−orbit splitting of $2p_{3/2}$ and $2p_{1/2}$..

In the V 2p spectrum (**Figure S5b**), two major peaks are V $2p_{3/2}$ and V $2p_{1/2}$ with binding energies at 516.73 and 524.12 eV, implying the formation of a V_2O_5 phase in the nanocomposite matrix.

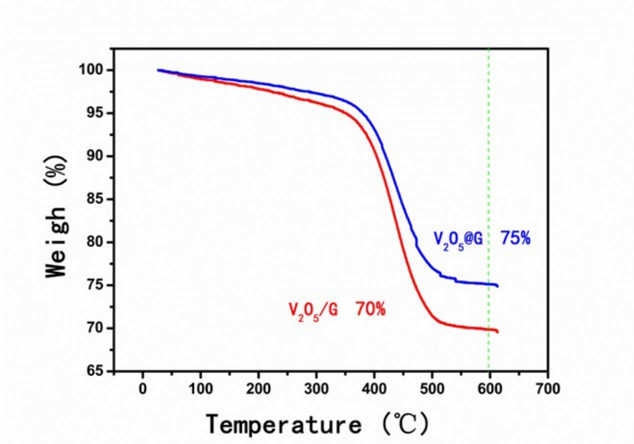

Figure S6. TGA of V_2O_5@G and V_2O_5/G. The TGA analysis was conducted in air using a heating rate of 10 ℃ min^{-1}. The weight loss from room temperature to 200 ℃ was mainly due to the removal of the physisorbed and chemisorbed water.

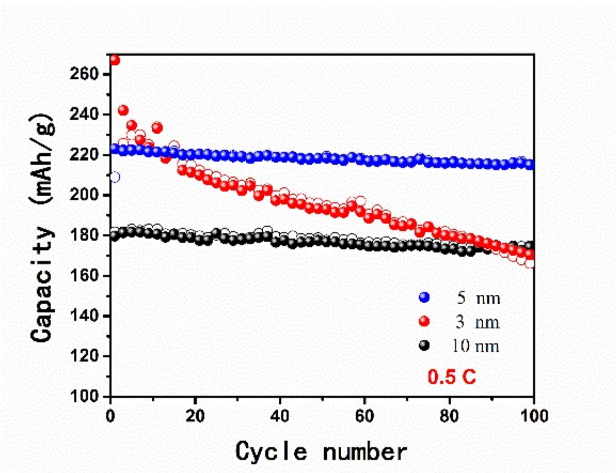

Figure S7. Different cycle performance of V_2O_5@G with different thickness of graphitic carbon coating via different CVD time (3.5 min, 5 min and 7 min respectively).

We also have in detail carried out the cycling performances of the resulting materials with different thickness of carbon coating via different CVD time (3.5 min, 5 min and 7 min, respectively). As shown in Figure S7, the 3 nm carbon coating thickness results in relative low cycling stability probably due to the inefficient electron transport network formation. When the coating thickness is 10 nm, the capacity of the whole electrode will be decreased due to the increase of the inactive carbon layers.

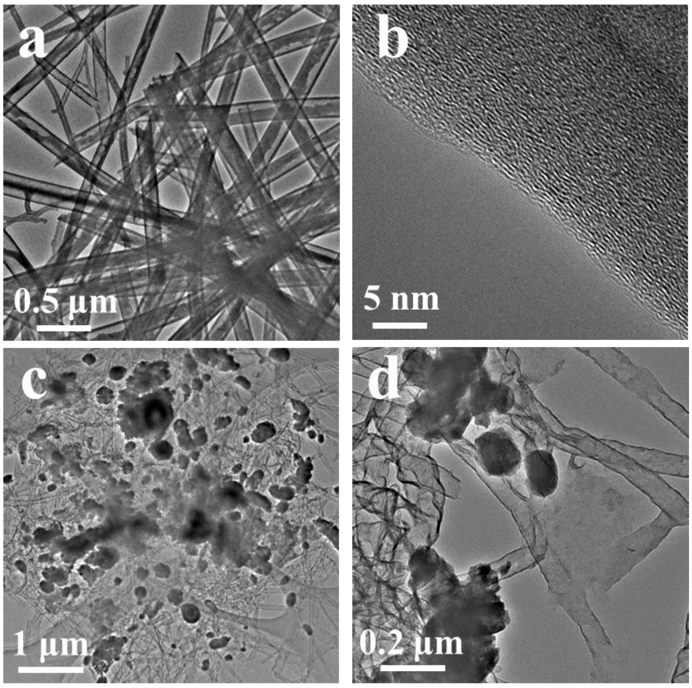

Figure S8. TEM images of V_2O_5@G after 100 cycles. (a) Scale bar, 500 nm. (b) Scale bar, 5 nm; TEM images of V_2O_5/G after 100 cycles. (a) Scale bar, 1 μm. (b) Scale bar, 200 nm;

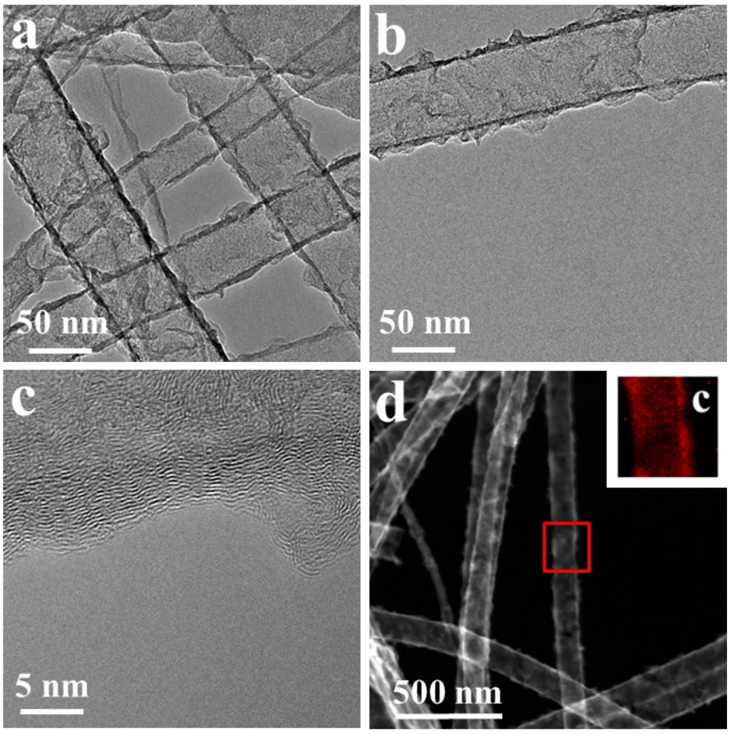

Figure S9. The TEM results of the sample after annealing to 1070℃ without the presence of V source. (a) The TEM photos. scale bar, 50 nm; (b) The TEM photos. scale bar, 50 nm; (c) The

TEM photos. scale bar, 5 nm; (d) Dark field transmission electron microscopy image. Scale bar, 500 nm; the inset is the Carbon elemental mapping of a selected area of above sample.

REFERENCE

1. N. K. You, Y. C. Kang and S. B. Park, *Nanoscale*, 2013, **5**, 8899-8903.
2. L. Mai, F. Dong, X. Xu, Y. Luo, Q. An, Y. Zhao, J. Pan and J. Yang, *Nano Lett.*, 2013, **13**, 740-745.
3. Y. Yang, L. Lei, H. Fei, Z. Peng, G. Ruan and J. M. Tour, *ACS Appl. Mater. Interfaces*, 2014, **6**, 9590-9594.
4. Y. Xu, M. Dunwell, L. Fei, E. Fu, Q. Lin, B. Patterson, B. Yuan, S. Deng, P. Andersen and H. Luo, *ACS Appl. Mater. Interfaces*, 2014, **6**, 20408-20413.
5. R. Yu, C. Zhang, Q. Meng, Z. Chen, H. Liu and Z. Guo, *ACS Appl. Mater. Interfaces*, 2013, **5**, 12394-12399.
6. X. F. Zhang, K. X. Wang, X. Wei and J. S. Chen, *Chem. Mater.*, 2011, **23**, 5290-5292.
7. H. B. Wu, A. Pan, H. H. Hng and X. W. Lou, *Adv. Funct. Mater.*, 2013, **23**, 5669-5674.
8. Y. Z. Zheng, H. Ding, E. Uchaker, X. Tao, J. F. Chen, Q. Zhang and G. Cao, *J. Mater. Chem. A*, 2015, **3**, 1979-1985.
9. Y. Li, J. Yao, E. Uchaker, J. Yang, Y. Huang, M. Zhang and G. Cao, *Adv. Energy Mater.*, 2013, **3**, 1171-1175.
10. A. Pan, T. Zhu, H. B. Wu and X. W. Lou, *Chem. Eur. J.*, 2013, **19**, 494-500.
11. M. Yan, F. Wang, C. Han, X. Ma, X. Xu, Q. An, L. Xu, C. Niu, Y. Zhao and X. Tian, *J. Am. Chem. Soc.*, 2013, **135**, 18176-18182.
12. A. Q. Pan, H. B. Wu, L. Zhang and X. W. Lou, *Energy Environ. Sci.*, 2013, **6**, 1476-1479.
13. H. Liu and W. Yang, *Energy Environ. Sci.*, 2011, **4**, 4000-4008.
14. A. Pan, H. B. Wu, L. Yu and X. W. Lou, *Angew. Chem. Int. Ed.*, 2013, **125**, 2226–2230.
15. D. Chao, X. Xia, J. Liu, Z. Fan, C. F. Ng, J. Lin, H. Zhang, Z. X. Shen and H. J. Fan, *Adv. Mater.*, 2014, **26**, 5794-5800.
16. W. Changzheng, F. Feng and X. Yi, *Chem. Soc. Rev*, 2013, **42**, 5157-5183.
17. L. Jun, Z. Yichun, W. Jinbin, P. Yong and X. Dongfeng, *Chem. Commun.*, 2011, **47**, 10380-10382.